Eur. Phys. J. B **35**, 3–12 (2003)
DOI: 10.1140/epjb/e2003-00250-0

THE EUROPEAN PHYSICAL JOURNAL B

Dynamic susceptibility of reentrant Fe-rich inhomogeneous amorphous alloys

F. Fernandéz Barquín[1,a], J.C. Gómez Sal[1], P. Gorria[2], J.S. Garitaonandia[3,b], and J.M. Barandiarán[3]

[1] Departamento CITIMAC, F. Ciencias, Universidad de Cantabria, Santander 39005, Spain
[2] Departamento de Física, Universidad de Oviedo, Oviedo 33007, Spain
[3] Dept. Elec. y Electrónica, F. Ciencias, Universidad del País Vasco, Bilbao 48080, Spain

Received 11 March 2003 / Received in final form 13 May 2003
Published online 22 September 2003 –

Abstract. Melt-spun amorphous alloys of $Fe_{91}Zr_9$, $Fe_{91}Zr_7B_2$, $Fe_{90}Zr_7B_3$ and $Fe_{88}Zr_8B_4$ have been characterized by AC susceptibility at frequencies between 30 Hz and 10 KHz. The measurements reflect the existence of reentrant spin glass transitions below 40 K for all cases. The transition shift per frequency decade is large compared to the observed in conventional spin-glass alloys. The shift value increases with the boron content and becomes closer to values in fine-particle systems. We find that the relaxation in $Fe_{91}Zr_9$ follows a critical slowing down at the reentrant transition, with exponents $z\nu = 7.2$ and $\beta = 0.7$. The non-linear susceptibility displays a peak at the transition in this alloy, but wider than in canonical spin glasses. A Vogel-Fulcher (VF) activation process can explain the frequency variation in all the Fe-Zr-B alloys. The reduction of the ideal glass temperature in the VF approach, found in the higher Boron content alloys, is an indication of a superparamagnetic-like behavior. The behavior shown by these alloys is intermediate between a collective freezing and superparamagnetic-like relaxation. We propose that this is arising due to a heterogeneous spin structure. The inclusion of a reduced amount of B, affects the magnetic spin structure.

PACS. 75.50.Lk Spin glasses and other random magnets – 75.50.Kj Amorphous and quasicrystalline magnetic materials – 75.40.Gb Dynamic properties (dynamic susceptibility, spin waves, spin diffusion, dynamic scaling, etc.)

1 Introduction

Reentrant spin glass (RSG) alloys are characterized by magnetic relaxation and irreversibility phenomena, when entering into the low temperature spin-glass state from a ferromagnetic arrangement. Such a spin-glass state (*cluster glass*) is usually visualized as a number of magnetic clusters randomly disposed in a metallic matrix, in which long-range RKKY interactions are present [1,2]. This situation is similar to that of *canonical* spin-glasses (SG), in which *randomly isolated individual* magnetic moments are dispersed in the matrix. The term cluster is thus described as an ensemble of limited number magnetic moments, coupled together by a ferromagnetic interaction. The critical slowing down observed close to the reentrant temperature (T_{RSG}), presents a difficult quantitative evaluation in RSG alloys in comparison to canonical spin-glasses, as it is affected by the behavior of ensembles of atoms, which may vary in size and, hence experimental results are relatively ill-defined. Progress is currently achieved by combining results gathered in amorphous and crystalline systems (more or less magnetically concentrated) [3]. Very recently, with the discovery of Giant magnetoresistance (GMR) in fine-particle nanometric systems of granular metals and the need of their detailed magnetic characterization, a complementary field to study the irreversibility phenomena is steadily growing. In these latter systems, magnetic particles of a few nanometers in size are present in a metallic matrix, with a non-magnetic behavior. Depending on the temperature, anisotropy and characteristic measuring time, they may experience the blocking or unblocking of the particle net moment, giving rise to similar macroscopic features to RSG systems in experimental techniques such as dc-magnetization (M_{DC}) and AC-susceptibility (χ_{AC}) [4]. This is at present an attractive debate as, in essence, these fine particle alloys are interacting grain ensembles, involving not tenths but thousands of atoms per nanometric grain [5,6]. By contrast, *ideal* (non-interacting) superparamagnetic systems are also constituted by single domain particles, but oscillating long-range RKKY interactions are absent.

Among the RSG compounds, Fe-rich Fe-Zr amorphous alloys constitute one of the first and paradigmatic systems

[a] e-mail: barquinl@unican.es
[b] *Present address*: Dept. Física Aplicada, F. Ciencias, Universidad del País Vasco, Bilbao 48080, Spain

since the early 80s [7]. In a relatively narrow compositional range, with a high concentration of the magnetic atom (Fe content > 80% at), SG, RSG and simple ferromagnets are found. These Fe-Zr amorphous alloys display striking magnetic behaviors including, the reduction of magnetic moment with increasing Fe-concentration, large high- field susceptibility at low temperatures, double-peaked hyperfine distributions derived from Mössbauer spectroscopy, high temperature resistivity minima, or exceptional magnetovolume effects and strong dependence of Curie temperature on mechanical stress, among others. These have given rise to a steady flow of studies [8–23], using different techniques for their structural and magnetic characterization. The basic fascination of this system (and similar Fe alloys with late transition metal elements, such as binary Fe-Y [24], Fe-Sc [25], Fe-Hf [26], or ternary alloys [27–30]) stems from the competition between magnetic interactions in metallic systems of high Fe-concentration (close to the Fe-percolation limit). In general terms, the Fe_xZr_{100-x} ($88 \leq x \leq 93$) amorphous alloys are known to be weak ferromagnets [10]. As commented above, the inclusion of small quantities of B-atoms in (to form the Fe-Zr-B alloys) or minute quantities of Fe-bcc nanograins do not alter enormously the reentrant behavior.

On the other hand, small additions of B-atoms during the synthesis process of the amorphous alloys and further appropriate thermal treatments result in nanocrystalline Fe-Zr-B (Cu) materials, which have gathered enormous attention for potential applications due to their extremely high susceptibility and low coercivity response [31–34]. The nanocrystalline state consists of bcc-Fe nanocrystals (≅10 nm) embedded in an amorphous matrix impoverished in Fe respect to the initial amorphous material. The interplay among the interaction of nanocrystalline grain through the exchange coupling, the grain boundaries and the remaining amorphous matrix is the basis of the remarkable decrease of coercivity. Changes in the magnetic behavior can be explained by structural (size of crystals and volume fraction) and magnetic (anisotropy and exchange correlation) parameters, and are described in references [31–34]. Recent studies of Fe-Zr-Cu-B alloys in the early stages of nanocrystallization, where a small fraction of bcc-Fe-nanocrystals is present, have shown the existence of magnetic relaxation phenomena at $T < 50$ K [35]. It is then plausible to anticipate that both structural arrangements, amorphous [36] and slightly nanocrystallized [35], should be related if the magnetic behavior appears to be so close.

Up to now different models have been proposed in order to explain such a complex magnetic behavior in Fe-Zr alloys. Some of them deal with a freezing of transverse moment components (for $T < T_{\rm RSG}$) [18] caused by the existence of randomly distributed antiferromagnetic interactions between Fe-atoms. Alternatively, other models claim for the existence of spin clusters or inhomogeneities with either regions of Fe-rich areas in low-spin state compared to the matrix (being the Fe-atoms in this latter in a high-spin state) [13,37] or local density variations in a chemically homogeneous environment [11]. Both viewpoints put forward the presence of indefinite regions of dubious size limits, where spin frustration is found, and consequently spin glass freezing transitions might be detected. Additionally, superparamagnetic effects have already been described for nanocrystalline materials of Fe-bcc grains, when the amorphous matrix is no longer magnetic (*i.e.* at $T > T_c$) and the relaxation of the magnetic moments in the grains is controlled by their size and anisotropy [38].

The different aspects exposed above and recently reported [34–36] findings in the Fe-Zr-B system strongly support the need of further effort, which is presented here. Through an adequate selection of four Fe-Zr-B amorphous alloys, the compositional crossover region between SG and RSG behaviors (between $Fe_{93}Zr_7$ and $Fe_{91}Zr_9$, see Ref. [8]) can be studied. This permits to explore what manifestations are characteristic of the magnetic relaxation of these magnetically concentrated alloys.

Since the very beginning and due to its sensitivity to detect and follow in detail dynamical magnetic processes, AC Susceptibility (ACS) has been employed to define the magnetic phase transitions in similar alloys [12,15,22,39]. To accomplish the above mentioned task, we have undertaken a systematic ACS study, which also fills in a gap of relatively uncommon analyses dealing with the frequency dependent reentrant systems.

2 Experimental

Ribbons of $Fe_{91}Zr_9$ (Fe91) and $Fe_{91}Zr_7B_2$ (B2) $Fe_{90}Zr_7B_3$ (B3) and $Fe_{88}Zr_8B_4$ (B4) were melt-spun in Ar-atmosphere after preparing the master alloy in an arc-furnace. Typical ribbon cross section is 1.5 mm wide and 0.02 mm thick. X-ray diffraction showed no crystallinity in either ribbon faces. Annealed samples of some compositions have also been prepared in order to compare to the as-quenched alloys. The time and temperature (1 hour, 400 K) of the annealing is well below the onset of the crystallization process (around 600 K). AC susceptibility ($\chi_{\rm AC}$) was measured at several frequencies between liquid helium temperature and 310 K at a steady rate of 0.1 K/min, allowing the instantaneous recording of the in-phase (χ') and 90°-quadrature (χ'') components. A high number of frequencies between $\nu = 0.03$ and 10 Khz was employed. For some particular cases susceptibility curves at $h = 0.1$ Oe field were additionally recorded. The direction of the oscillating h field was longitudinal to the sample plane (pieces of ribbon stacked together) to minimize the effect of demagnetizing fields and eddy currents. Non-linear coefficients of the AC susceptibility were simultaneously obtained by measuring the harmonics of the induced secondary signal with a usual lock-in detection.

3 Analysis of the AC susceptibility

3.1 General behavior of the AC susceptibility

In this section a common methodology in the analysis of reentrant systems is followed [2]. Firstly, the results

are evaluated showing the reentrant behavior and defining the compositional tendencies of susceptibility, Curie and reentrant temperatures. On a second step, the reentrant transition is studied in detail and the distribution of relaxation times is estimated through an expression related to the Cole-Cole framework. Finally, the evaluation of the kinetics of the transition is studied in terms of the current theories.

Figure 1 shows the thermal variation of ACS susceptibility at 10 KHz of all the alloys. The real component of susceptibility (χ') grows rapidly with increasing temperature, showing a visible knee, marked as $T_{\rm RSG}$. Then it stabilizes, in a characteristic demagnetization-limited ferromagnetic behavior, and afterwards falls down at the Curie temperature, well above 150 K. The curves are similar to the low-field DC magnetization ($M_{\rm DC}$) measurements in similar alloys [36]. The magnitude of χ' increases with the increasing boron content. Alternatively, the out-of-phase component (χ''), approximately 10% of the in-phase component, shows firstly, a low temperature peak below 30 K. Then there is a signal more or less flat and finally, a marked decrease of signal when approaching $T_{\rm c}$. The two magnetic transitions corresponding to the ferromagnetic-spin glass (reentrant transition, $T_{\rm RSG}$) and the ferromagnetic-paramagnetic transition ($T_{\rm c}$) reported in Fe-Zr (Fe-rich) [8] and in Fe-Zr-B alloys [36,40,41] are clearly defined in our ACS results. This state is clearly affected by the magnitude of the coercive field of each sample and then could change as a function of the driving field.

In Figure 2, a comparison between the curves obtained at 1 Oe and 0.1 Oe driving h fields is shown for Fe91. Similar values of susceptibility are observed for both oscillatory fields, being the shape relatively similar between the two. For Fe91, where the weaker susceptibility values are found, the $h = 1$ Oe, is not large enough to fully magnetize the ribbons and this is reflected from a relatively flat signal in χ''. For B3 and B4, with larger susceptibility and $T_{\rm c}$ values, that oscillating field is sufficient to drive the sample closer to saturation, masking the response at $T_{\rm RSG}$ and $T_{\rm c}$. As it has been pointed out recently for Fe-Ni-P-B-Al reentrant amorphous alloys [42], the control of the magnitude of the driving field h should be taken into account to obtain a good definition of the transition. In our case, the geometry enhances the definition of the χ'' peaks, and the variation of the low-temperature relaxation peak position with h is small. For the low field $h = 0.1$ Oe data the signal in the transitions (especially the $T_{\rm RSG}$) is somewhat better resolved. However, given the higher signal to noise ratio in the susceptibility of the 1 Oe curves, we prefer to use the data for this latter excitation field throughout this work.

The temperatures of transitions are close in annealed and as-quenched samples. Results are presented in Figure 3, as an example for B2. This is especially evident (see Fig. 3) in the low-temperature magnetic transition (extremely sensitive to any change). Similar observations related to annealing effects had been already observed for pure Fe-Zr alloys [21]. This is a crucial finding meaning

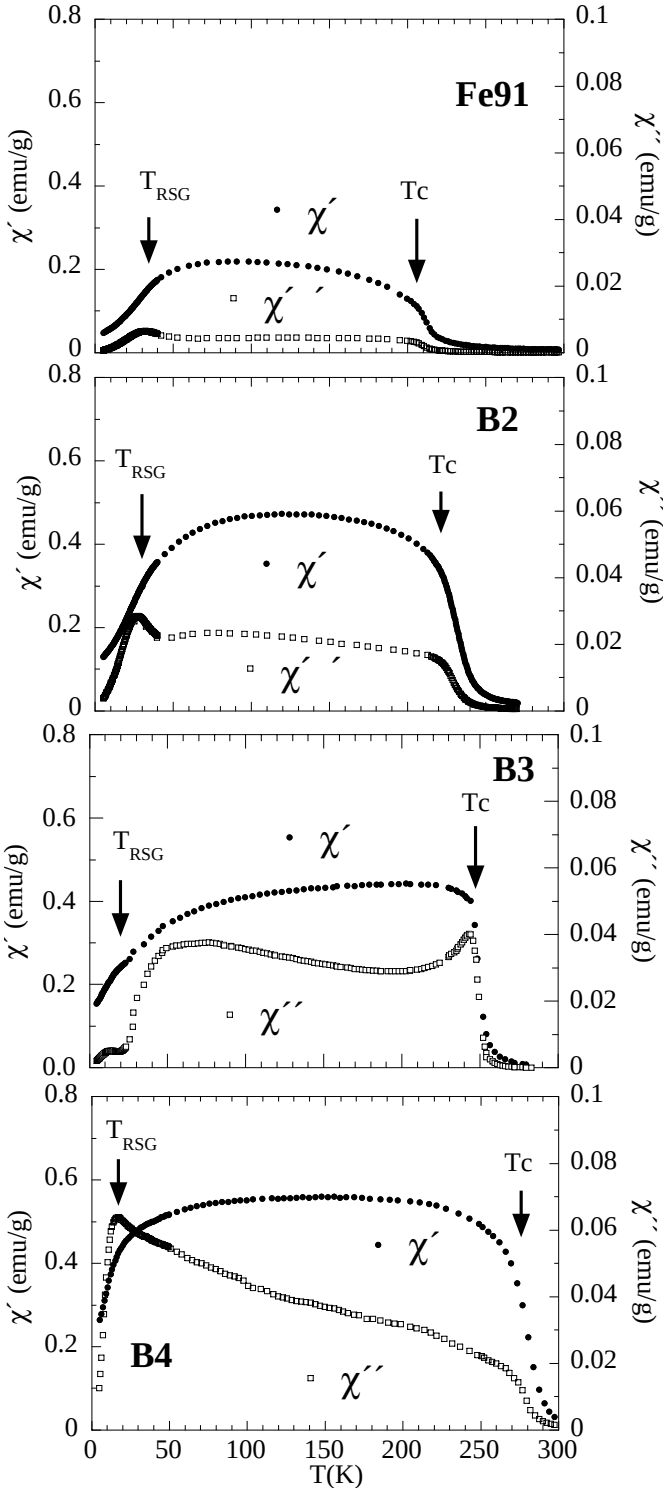

Fig. 1. ACS ($h = 1$ Oe) plot showing in phase (χ') and out of phase (χ'') components for a single frequency $\nu = 10$ KHz of all the alloys (Fe91 = $Fe_{91}Zr_9$, B2 = $Fe_{91}Zr_7B_2$, B3 = $Fe_{90}Zr_7B_3$, B4 = $Fe_{88}Zr_8B_4$) in as-quenched state. The susceptibility increases when the B-content is increased as found in reference [36] from $M_{\rm DC}$ magnetization. Arrows mark T_c and $T_{\rm RSG}$ of the four alloys according to the susceptibility derivative ($d\chi'/dT$) and the maximum in $\chi''(T)$, respectively. Note the increase of T_c and the tendency to decrease of $T_{\rm RSG}$ with increasing B content. Data points have been skipped for clarity.

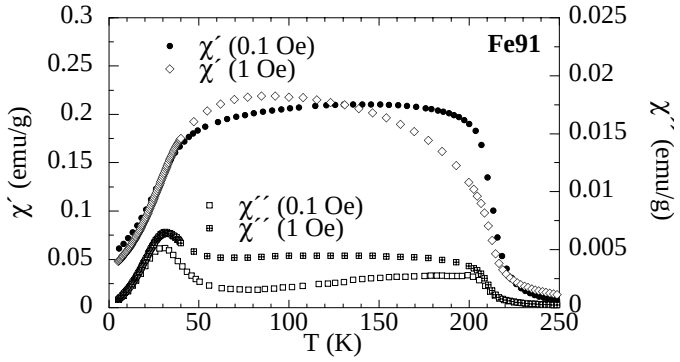

Fig. 2. Variation of ACS (χ' and χ'') for the $Fe_{91}Zr_9$ (Fe91) alloy with oscillating fields ($h = 1$ and 0.1 Oe). Only one frequency ($\nu = 0.1$ KHz) has been depicted. The positions of T_c and $T_{\rm RSG}$ appear at similar temperatures.

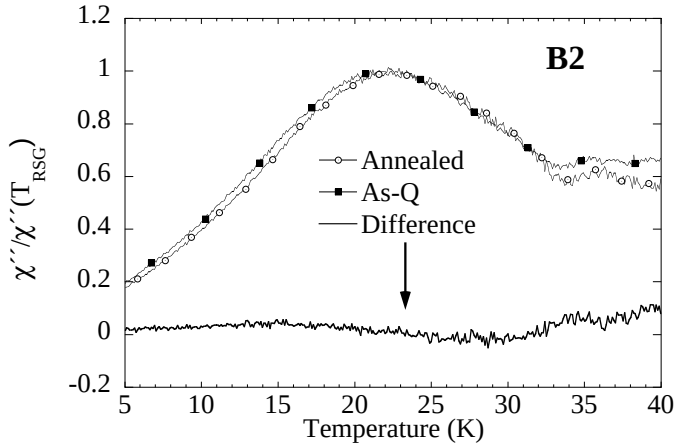

Fig. 3. The complex AC susceptibility of annealed and as-quenched $Fe_{91}Zr_7B_2$ alloys ($h = 1$ Oe). For clarity, measurements at $\nu = 0.1$ KHz have been included uniquely. Note that normalized curves [by the $\chi''(T_{\rm RSG})$ value] are absolutely similar and the difference between them is negligible.

that the experimental features are intrinsic to the samples and not an artefact due to the fabrication process, as quenched internal stress or compositional inhomogeneities produced by the rapid cooling. Due to the selected annealing temperature (much lower than the crystallization one), the structural rearrangements are restricted to the elimination of the excess free volume and homogenization of the amorphous phase. These do not modify significantly the reentrant transition temperature, being a clear sign of the intrinsic magnetic disorder in the spin structure of the alloys.

The Curie temperatures are evaluated as the inflection point of the χ' curve in the high temperature region ($T > 150$ K). As expected, Curie temperatures are frequency independent (within the error limits) in the studied range. Our results calculated from the minimum in the real susceptibility derivative ($d\chi'/dT$) (see Fig. 4 in which only B3 is shown) are in Table 1. These temperatures are close to values obtained from $M_{\rm DC}$ [36,43].

A complementary path is to employ the Kouvel-Fisher (KF) analytical method [44], which provides a numerical value of γ (critical exponent of the susceptibility in a ferromagnetic-paramagnetic transition). In the KF analysis, the zero field susceptibility (χ_0) behaves, close to T_c as:

$$Y(T) = \left[\frac{d\ln(1/\chi_0)}{dT}\right]^{-1} = \frac{T}{\gamma} - \frac{Tc}{\gamma}. \qquad (1)$$

A plot of $Y(T)$, shown in Figure 4 for B3 as an example, gives values for γ and T_c from the slope and intercept, respectively. Note that T_c in B4 (279 K, see Tab. 1) is very close to the experimental upper temperature limit and the obtained values are not reliable. The values have been inserted in Table 1. The extrapolation to obtain T_c from equation (1) can be disturbed by the demagnetizing factor (N) of the samples, that imposes a limiting value of $\chi \approx 1/N$ at the transition. This can explain the difference with the values of T_c obtained from the $d\chi'/dT$.

Table 1. T_c (Der): Values of the Curie temperature T_c (in Kelvin) from the derivative of susceptibility. T_c (KF): T_c (in Kelvin), and γ, critical exponent, derived from the Kouvel-Fischer (KF) analysis in the $|T - T_c|/T_c \leq 0.15$ region. $T_{\rm RSG}$: reentrant temperatures taken from χ'' at $\omega\tau = 1$ at 1 KHz.

Alloy	T_c (Der)	T_c (KF)	γ	$T_{\rm RSG}$
$Fe_{91}Zr_9$ (Fe91)	211(1)	206(6)	1.02(4)	28.4(1)
$Fe_{91}Zr_7B_2$ (B2)	223(1)	210(4)	1.09(2)	24.0(1)
$Fe_{90}Zr_7B_3$ (B3)	248(1)	244(1)	1.64(4)	10.3(1)
$Fe_{88}Zr_8B_4$ (B4)	279(1)			14.2(1)

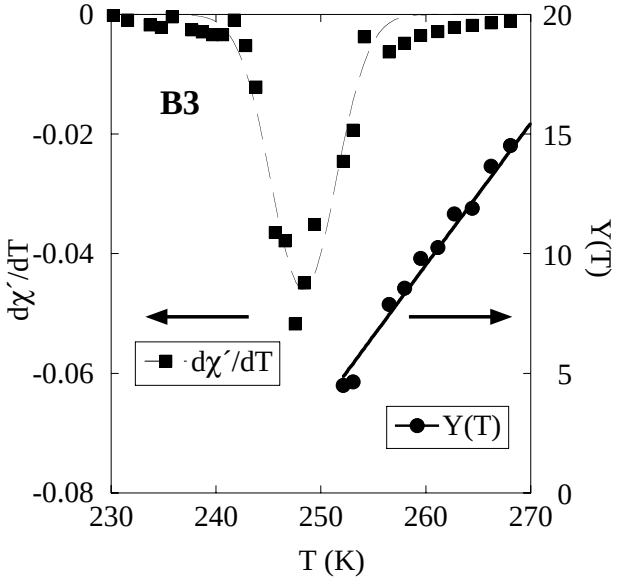

Fig. 4. Thermal variation of the derivative of χ', yielding a value of $T_c = 248$ K, and Y, as defined in equation (1) from the Kouvel-Fischer analysis, for B3 at $h = 1$ Oe and $\nu = 1$ KHz. The straight line is a fit to obtain the values of the critical exponent $\gamma = 1.64$ (inverse slope of $Y(T)$) and T_c(KF) = 244 K, from the temperature intercept.

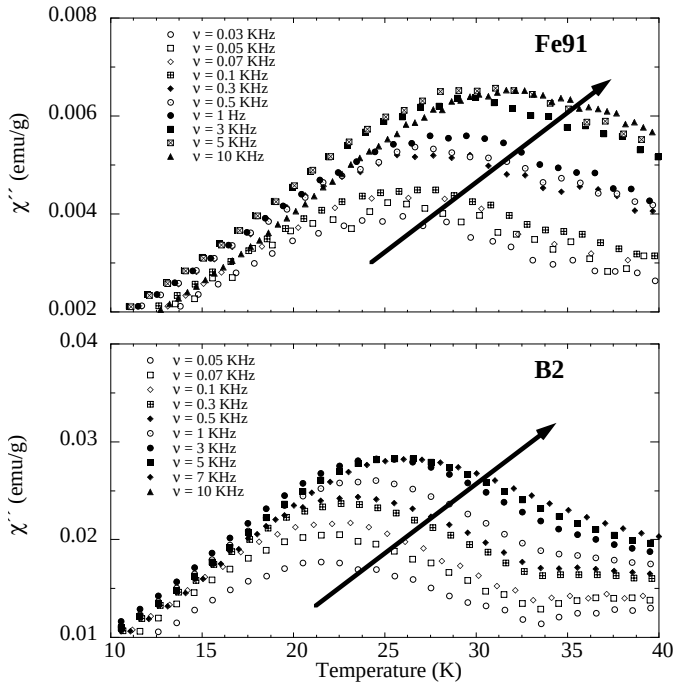

Fig. 5. Comparison in the same temperature range of the thermal shift of $\chi''(\nu)$ maxima at low temperatures between Fe91 and B2. The magnitude of $\chi''(\nu)$ tends to increase with increasing frequency. Only 10% of data points is shown for each frequency.

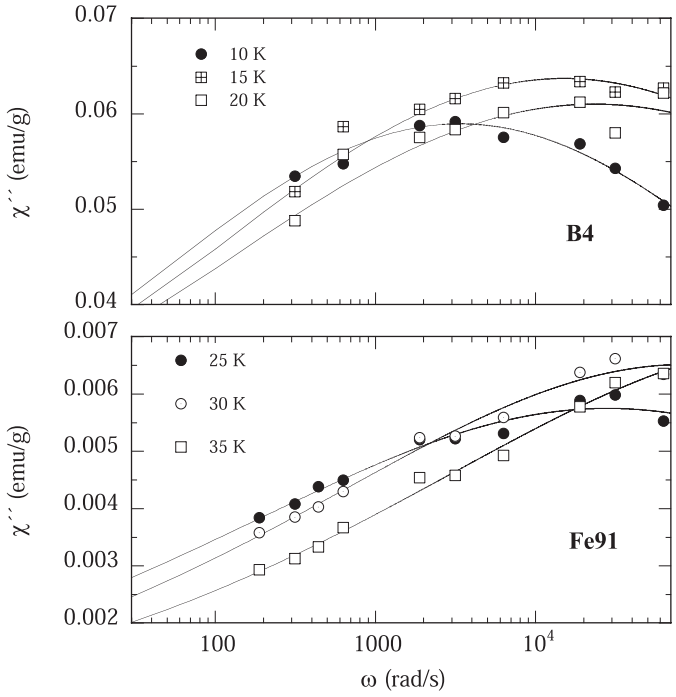

Fig. 6. Fittings of $\chi(\omega = 2\,\pi\,\nu)$ according to Eq (2) for the Fe91 and B4 alloys at different temperatures around the freezing transition. The $\Delta = 0.8$ (see Eq. (3)) is also found in random anisotropy amorphous alloys with spin inhomogeneity in the magnetic arrangement.

Nevertheless T_c values obtained by both methods show a similar trend.

The drastic increase of T_c and the magnitude of susceptibility with boron content reflect a large enhancement of their ferromagnetic character; band structure modifications have been invoked to explain such features [36]. Our estimated γ-coefficients show values similar to the calculated in 3d-Heisenberg ferromagnets ($\gamma = 1.4$) [45], for the *most* FM sample, B3, and is not far to amorphous $Fe_{90}Zr_{10}$ ($\gamma = 1.35$). By contrast, Fe91 and B2 show γ-values similar to crystalline RSG $Fe_{54}Ni_{26}Cr_{20}$ ($\gamma = 0.92$) [46], lower than reported in other studies [47], as a result of their especially weak ferromagnetic character.

3.2 Relaxation at the reentrant transition: distribution of relaxation times

The ACS measurements obtained at the reentrant transition, are able to determine more precisely the nature and kinetics of the effect. In Figure 5, enlarged plots are shown for Fe91 and B2 in the same temperature range. The observed frequency shift of the maxima of χ'' is a clear sign of the existence of relaxation phenomena in the reentrant transition of the compounds, as already reported for $Fe_{90}Zr_{10}$ [22]. The shift can also be calculated from the inflection point of the real component χ' turning out that both observations give the same results.

The relaxation of magnetic moments usually follows a distribution of times $g[\ln(\tau)]$ which can be quantitatively obtained by using an expression based on the well-known phenomenological Cole-Cole model in the analysis of ACS curves [2]. In particular, the corresponding $g[\ln(\tau)]$ is [48]:

$$g\left\{\ln(\tau_c)\right\} = \frac{1}{2\pi}\frac{\sin(\Delta\pi)}{\cosh\left[(1-\Delta)\ln(\tau/\tau_c)\right] - \cos(\Delta\pi)}. \quad (2)$$

This quasi-Gaussian distribution of times is defined by the width represented by $\Delta(0 \leq \Delta \leq 1)$ and is centered at $\ln\tau_c$. The expression (2) can be used to obtain a variation for $\chi''(\nu)$ according to:

$$\chi''(\omega) = A\left\{\frac{\cos\left(\frac{\Delta\pi}{2}\right)}{\left[\cosh\left((1-\Delta)\ln(\omega\tau_c)\right)\right] + \sin\left(\frac{\Delta\pi}{2}\right)}\right\} \quad (3)$$

in which $\omega = 2\pi\nu$ is the angular frequency and A is a pre-factor related to the susceptibility. It is possible to fit the ACS curves using such a distribution, as it is shown for Fe91 and B4 in Figure 6. Large values of $\Delta(\approx 0.8)$ are signs of a broad distribution in both cases and the use a complete Cole-Cole analysis should be avoided [2]. This is not surprising in these reentrant alloys considering the high inhomogeneity in their spin arrangement, already pointed out throughout the introduction. In this way, it is more convincing to analyze our data assuming that the transition is well defined by the maximum in $\chi''(\nu)$, in which we take $\omega\tau = 1$. The $T_{\rm RSG}$ values, dependent on the frequency, are shown at 1 KHz in Table 1 for all the

alloys. There is a tendency to decrease with increasing B-content.

An extremely interesting parameter is the observed relative $T_{\rm RSG}$ shift (δ_T), evaluated as: $\delta_T = \Delta T_{\rm RSG}/\big(T_{\rm RSG}\Delta\log(\omega)\big)$. This value is 0.066(3) for Fe91, 0.095(6) for B2, 0.121(5) for B3 and 0.14(1) for B4. Normally, paradigmatic metallic systems with a spin glass transition (AuMn, AgMn, AuFe) present much lower values between 0.004-0.002 [2]. The $T_{\rm RSG}$ shift values for Fe-Zr-B alloys increase with the addition of Boron, becoming closer to values of superparamagnetic (fine particle) compounds, theoretically around $\delta_T = 0.1$ [4]). This finding is a clear indication of the different relaxation process between our alloys and the canonical spin glasses. The lowest shift is observed in $Fe_{91}Zr_9$. We will present in the following an analysis to ascertain the nature of its relaxation mechanism.

3.3 Reentrant transition in amorphous $Fe_{91}Zr_9$: critical slowing down

The SG alloys should display a conventional critical (dynamic) slowing down behavior. In this approach, the critical behavior is expected at a characteristic temperature in which the transition relaxation diverges. The relaxation time for the decay of the fluctuations τ is related to the spin correlation length ξ according to $\tau \propto \xi^z$. The expression for τ is given by [2].

$$\tau = \tau_0 \left(\frac{T}{T_0} - 1\right)^{-z\nu} \tag{4}$$

in which T_0 is the transition temperature, τ_0 is the relaxation time of the individual moments and $z\nu$ is a critical exponent. The analysis gives a best combination for $z\nu = 7.2$, $T_0 = 20.5$ and $\tau_0 = 10^{-8}$ s and the result is depicted in the inset of Figure 7. The $z\nu$ value is inside a general behavior reviewed by Souletie and Tholence ($5 < z\nu < 11$) [49], usually labeled as "fragile regime". Some authors consider that the variations in these values might reflect an absence of a true critical exponent [50]. In comparison to more recent data, the critical exponent $z\nu$ is similar to $Fe_{80}Mn_{10}Zr_{10}$ ($z\nu = 6.5$) [39], and $Fe_{90}Zr_{10}$ ($z\nu = 8$) [22]. This value is also in agreement with values other RSG alloys such as amorphous Fe-Ni-P-B-Al ($z\nu = 7.9$) [42] close to nanocrystalline Fe-Nb-B ($z\nu = 6.9$) [51] and slightly lower than 5d-crystalline alloys such as U(Pd. Pt, Au)Si_3 [52] $z\nu \approx 10$. Overall, these values agree with the $z\nu = 7.9$ obtained through calculations by Ogielski [53] in a 3d Ising simulation, in contrast to the expected value $z\nu \approx 2$ in conventional phase transitions. Additionally, it is also expected [54] that in a transition to a spin-glass state, a dynamic scaling for the χ'' should also be found. Taking $\varepsilon = (T - T_0)/T_0$:

$$\chi''(\nu, T) = \varepsilon^{\beta} F(\nu\varepsilon^{-z\nu}). \tag{5}$$

Figure 7 shows the results the power-law scaling of χ'', using $\beta = 0.70(5)$. The result shows a reasonable scaling, with the curves collapsing on a universal curve. The

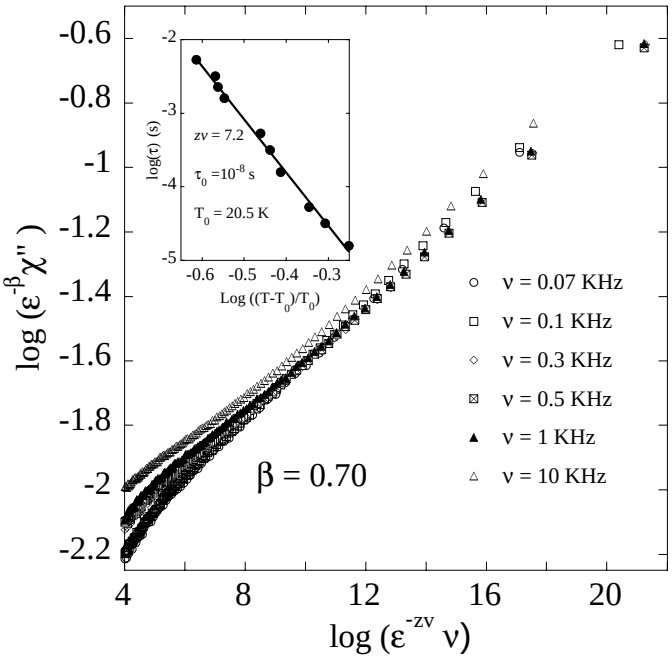

Fig. 7. Critical slowing down analysis of $\chi''(\omega, T)$ data at $T > T_{\rm RSG}$ (see Eqs. (4, 5)) of the $Fe_{91}Zr_9$ alloy. The complex susceptibility at different frequencies collapse on a master curve with $\beta = 0.7$. Inset: Analysis of the shift of the of $\chi''(\omega, T)$ maxima in the same framework. The straight line corresponds to the best fitting. The $z\nu = 7.2$ exponent is in excellent agreement with other RSG-amorphous alloys.

β value is close to the exponent ($\beta = 0.5$) obtained through Monte Carlo simulations [2].

Another experimental confirmation of the nature of this transition is given by the behavior of the non-linear susceptibility. The non-linear response of the magnetization M is described as a series of terms containing field powers, in an expansion:

$$M = M_0 + \chi_1 h + \chi_2 h^2 + \chi_3 h^3 + \cdots \tag{6}$$

where M_0 is the spontaneous magnetization, h the oscillating field $h = h_0 \sin\omega t$, and χ_1 the linear and $\chi_2, \chi_3 \cdots$ the non-linear susceptibilities. The non-linear susceptibility can be obtained from $M_{\rm DC}$ measurements with different applied fields but more directly from the harmonics in the ACS. For this latter technique, very recently Bhargava *et al.* [55] have given a detailed description of the equations involved.

In a ferromagnet, it is expected that all susceptibility terms contribute to the magnetization, and the appearance of a peak at the Curie point. For *true* spin glasses (absence of spontaneous magnetization), it is expected that only odd-power terms should appear to obey the inversion symmetry respect to the field [56]. Regarding the freezing transition, it has also been shown that the third harmonic corresponding to χ_3 (cubic susceptibility) should diverge $\big(\partial^3\chi_3/\partial h^3 \to \infty\big)$ at the freezing transition. In summary, if a spin glass transition is present, a featureless signal should appear in χ_2' and a peak should be clear in χ_3'. This is precisely what is observed in Figure 8 confirming

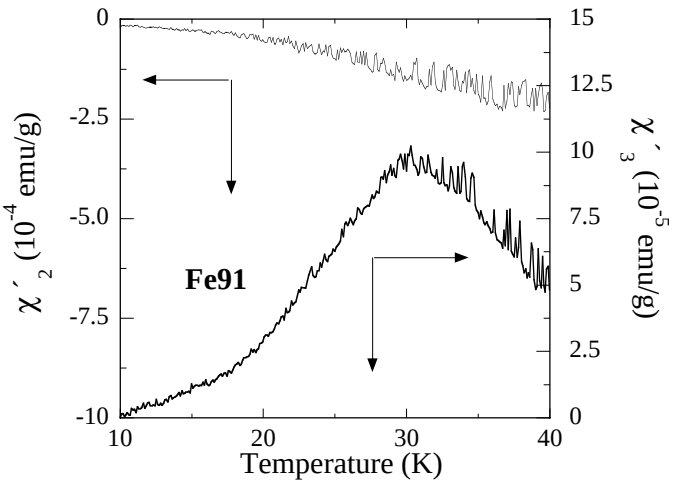

Fig. 8. Thermal variation of the non-linear susceptibility of the $Fe_{91}Zr_9$ alloy around the reentrant transition. A maximum in the third harmonic χ_3' is clearly observed at the spin-glass transition. A sharp divergence is only expected in the case of freezing of individual spins. The divergence is not visible in the second χ_2' harmonic.

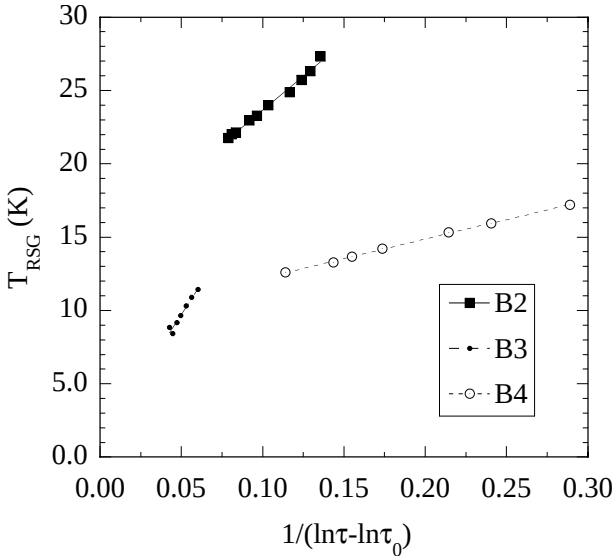

Fig. 9. Variation of $T_{\rm RSG}$ in a Vogel-Fulcher law dependence for the Fe-Zr-B alloys. Note the shift in the abscissa values due to different values of τ_0. Straight lines mark the fitting (see parameters in the text). The quality of fit is best for the B4 alloy ($R > 0.99$).

the existence of a spin-glass transition in the $Fe_{91}Zr_9$ alloy. The χ_3' peak is narrow in canonical spin-glasses [57], but as an effect of the existence of spin-clusters in the alloys, the observed peak presents a FWHM $\approx$ 10 K and a relative breadth $\sigma_{\rm REL}$ = FWHM/$T_{\rm max}$ $\approx$ 0.3, if a Gaussian shape is assumed. Non-linear susceptibility studies in freezing transitions are still scarce but a rough estimation can be presented taking data of amorphous SG $Fe_{93}Zr_7$ [15] $\sigma_{\rm REL} \approx 0.1$, whereas crystalline $Fe_{57}Ni_{23}Cr_{20}$ [46] and $Ce(Fe_{0.96}Al_{0.04})_2$ [58], with a similar RSG behavior to $Fe_{91}Zr_9$ (according to the ACS shape), both give $\sigma_{\rm REL} \approx 0.2$. This can just be indicative estimation but it is clear that, as a comparison, for an archetypal canonical spin glass of $Au_{96}Fe_4$, reported by Bitoh *et al.* [59], we have evaluated $\sigma_{\rm REL} \approx 0.05$, much lower than the values estimated above.

3.4 Analysis of the relaxation in the Fe-Zr-B alloys: activated dynamics

If a critical analysis is performed on these alloys, the fits give unrealistic values (for example, $z\nu = 3.2$ in B4), impossible to justify under a *true* spin-glass transition scheme. To discuss about the nature of the transition in amorphous Fe-Zr-B, it is necessary to use another approach. Especially B3 and B4 require another class of analysis of dynamic behavior. This can be the Vogel-Fulcher (VF) law for the relaxation process. This expression, of phenomenological nature, is common when analyzing dynamic effects in glassy or disordered systems. In particular, its validity has been reported in magnetic relaxations not only in RSG systems, but also in interacting nanoparticle GMR systems such as granular Co-Cu ribbons [60], Fe-Cu-Ag powders [6], among others have reported its validity. The VF for the relaxation time is:

$$\tau = \tau_0 \exp\left(\frac{E_a}{k_B(T - T_*)}\right) \qquad (7)$$

where, τ_0 is the attempt relaxation time, Ea, an activation energy, and T_* is called the "ideal glass" temperature [2]. If $T_* = 0$, this expression becomes the Arrhenius law, typical in non-interacting systems, as ideal superparamagnets. The VF analysis (see Fig. 9) provides a method to compare all the alloys in a single framework, yet purely phenomenological. The results for B2, B3 and B4 alloys present the following parameters: $Ea/k_B = 89 \pm 2$ K and $T_* = 14.7 \pm 0.2$ K ($\tau_0 \approx 10^{-8}$ s), $Ea/k_B = 170 \pm 6$ K, $T_* = 1.3 \pm 0.3$ K ($\tau_0 \approx 10^{-12}$ s), and $Ea/k_B = 26.5 \pm 0.7$ K, $T_+ = 9.6 \pm 0.1$ K ($\tau_0 \approx 5 \times 10^{-7}$ s), respectively. The compositional tendency of E_a and T_*, a decrease with increasing B-content, is closely related to the increasing weakness of the spin glass state, approaching the behavior of non-interacting systems. Moreover the quality of the fit tends to increase with the boron-content, and it is remarkable in B4. This alloy shows, consequently, a behavior totally different to critical slowing down.

4 Discussion

The intermediate character observed in the Fe-Zr-B transition, different to the critical dynamics found in $Fe_{91}Zr_9$, should be linked to a particular spatial spin arrangement. If we rewrite the alloys in approximate compositions $(Fe_{93}Zr_7)_{98}B_2$ (B2), B3 as $(Fe_{93}Zr_7)_{97}B_3$, and B4 $(Fe_{92}Zr_8)_{96}B_4$, it is clear that these melt-spun alloys belong to a compositional region where the Fe/Fe+Zr ratio

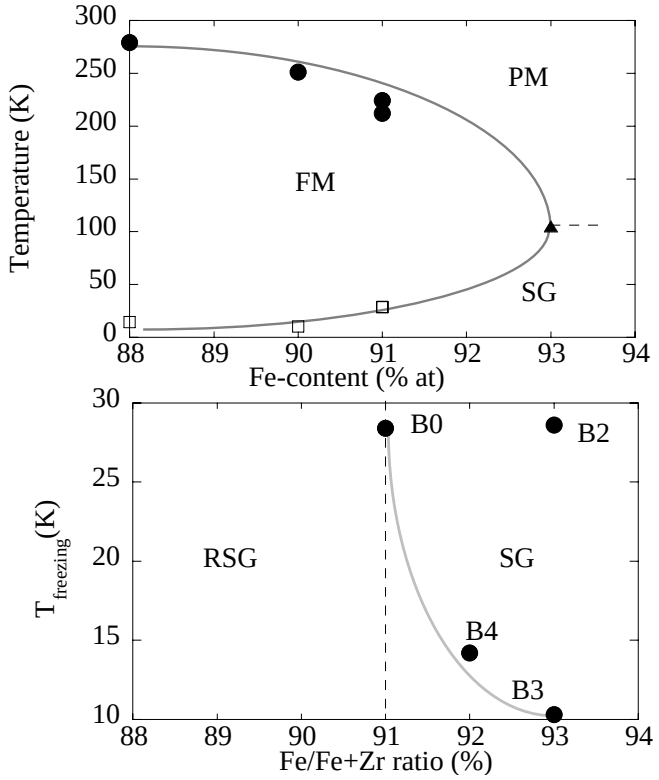

Fig. 10. Top: Magnetic phase diagram of the high-concentration Fe-Zr-B alloys as a function of the absolute atomic Fe-content: T_c are marked by (•) and freezing temperatures as (□). The value of the $Fe_{93}Zr_7$ (▲) is taken from reference [15]. Below: Variation of the freezing temperatures (•) as a function of the Fe/Fe+Zr ratio. Lines are only guides for the eyes.

is between the SG ($Fe_{93}Zr_7$) and RSG ($Fe_{91}Zr_9$) [8] (see Fig. 10). This figure helps to understand the reverse position of B3 and B4 respect to the $T*$ evolution in the VF analysis. On the other hand, B2 only shows a slight deviation towards the activated dynamics. In addition, the magnetic phase diagram (Fig. 10, top) resembles those of well-established reentrant amorphous alloys [8,25,30,61].

The spin-glass transitions are found in whenever the following conditions are fulfilled: i) competing magnetic interactions, and ii) site or bond disorder. In the case of Fe- Zr-B (Fe-rich) amorphous alloys the conditions to produce a reentrant behavior should be similar to those to the well known pure Fe-Zr (Fe-rich) alloys. As pointed out in the introduction, Fe-Zr alloy is believed to have an inhomogeneous spin structure, whose microscopic nature is still a question of controversy. The key issue is to define microscopically what the length scale of those spin inhomogeneities is. This controversy is parallel to the discussion found in recent reports dealing with crystalline materials such as Sm_2Fe_{17} [62], $FeCr_2S_4$ [63] or Rare Earth-Al_2 [64]. The experimental features in the ACS are similar to the ones presented above and explained by variations in the anisotropy and domain structure. However the very low anisotropy and the amorphous arrangement in the alloys analyzed here suggests other microscopic explanation. In this sense, some authors have put forward a model in which short-ranged antiferromagnetic interactions (contacts) are scattered throughout the amorphous ferromagnetic spin environment [18]. With this, competing interactions and site disorder conditions are both fulfilled and many experimental features and, especially, the variation of moment with Fe-concentration are well described. Others [11,13,65] invoke the existence of ferromagnetic spin clusters *in a matrix*.

For both points of view, it is still difficult to ascertain the experimental length scale of the spin inhomogeneities (either the antiferromagnetic contacts or clusters) even if *direct* powerful microscopic techniques are employed. In this sense, SANS under magnetic field of $Fe_{91}Zr_9$ (RSG) shows slight humps in the signal associated to spin inhomogeneities, but surface contributions from the flat ribbon surface might be present masking the results [19]. Very recently, muon spin relaxation has been successfully performed in $Fe_{92}Zr_8$ (SG) alloys showing the transverse freezing [23], but it is impossible to define the medium-ranged (at a mesoscopic scale) spin correlation lengths. Neutron (polarized and unpolarized) diffraction has also recently been reported in $Fe_{92}Zr_8$ and $Fe_{90}Zr_{10}$ (RSG) [66] and combined neutron and X-ray diffraction in $Fe_{91}Zr_9$ [67]. This latter reference also presents Reverse Monte Carlo modeling (RMC) to fit both types of spectra. The simulations (≈5000 atoms) carried out in a 4 nm box show that the inclusion of antiferromagnetic couplings between some of the Fe-atoms improves the fitting to the neutron magnetic and structural structure factor S(Q). However, it is not so clear the absence of nanometric size clusters as the length scale is limited precisely by the wide-angle diffraction data used in these simulations.

In the present case, the addition of boron in the Fe-Zr alloys produces the modification in the structure by the inclusion of B atoms itself. Additionally the amorphous alloys can be compared to the nanocrystalline alloys created from them. The B atoms tend to situate between the metallic ones thus increasing the ferromagnetic coupling. This is clearly reflected in a increase of the Curie temperature and the general enhancement of the FM character of the alloys.

At a local scale, B atoms also favor the appearance of clusters, which behave isolated from each other, if they are separated by distances larger than the exchange correlation length of the ferromagnetic matrix. The number of Boron atoms being very small, these cluster are consequently separated, as an average, long distances, and the magnetic relaxation is slower (*i.e.*: more superparamagnetic-like). This inhomogeneous arrangement is intrinsic and thermally stable, as deduced from the annealing results. In this sense, very recently, structural nanometer-scale defects have been characterized by transmission electron microscopy in bulk amorphous alloys [68].

On the other hand, there exist similarities in FeZrB(Cu) and FeNbCuSiB nanocrystalline alloys respect to the amorphous alloys analyzed here. In the

nanocrystalline alloys, nanometric crystallites are formed in a predominant amorphous matrix, giving rise to magnetic relaxation of the DC magnetization in ZFC-FC sequences [35]. These phenomena have been recently interpreted using simple structural models [35,69,70], involving the nanometric grains, partially coupled by the exchange interaction: Depending on the structural configurations, drastic variations in the coercive field are found. In the amorphous case presented here, the clusters are not so well-defined in size as is the nanocrystalline case giving rise to the observed magnetic relaxation behavior. Recently, Fe-oxides in insulating matrix [71] and Fe-C ferrofluids [72,73], with increasing interactions between particles, have been studied comprehensively showing precisely the opposite approach to that described here. The analysis of AC susceptibility in fine particle systems evidences that, for some concentrations, strong interparticle interactions are present. These latter give rise to a spin glass-like dynamics.

5 Conclusions

The AC-susceptibility measurements carried out in melt-spun amorphous alloys of $Fe_{91}Zr_9$ and Fe-Zr-B, precursors of soft nanocrystalline alloys, have revealed the existence of magnetic reentrant transitions at low temperatures, decreasing in temperature as the B content was raised. The parameters characterizing the transition in the $Fe_{91}Zr_9$ are similar to those reported in other reentrant systems, showing critical dynamics and a clear peak in the non-linear susceptibility. The peak width is sufficient large to confirm a cluster spin glass behavior, in a concentrated magnetic alloy.

The dynamics of the relaxation in the B-containing alloys is slower than conventional spin-glasses (especially in B3 and B4 alloys), resembling that of interacting superparamagnets, as deduced from the high T_{RSG} shift values and the absence of critical dynamics. These observations are also similar to other large anisotropy crystalline compounds, in which the role of pinning centres is discussed [62–64]. Here, in these low anisotropy amorphous alloys, there exists an inhomogeneous spin arrangement affecting the domain structure. Such a disordered arrangement at the nanoscopic scale is enhanced by the addition of B atoms in the Fe-Zr amorphous matrix, modifying the anisotropy at a local level. The intermediate character of these Fe-Zr-B alloys can be linked to a series of recent studies in a wide variety magnetic systems [5,6,30,51,65,69,74,75]. In these, the crossover between non-interacting superparamagnetism and strong interparticle interactions and, between spin-glass and reentrant behavior is undefined and object of extensive research effort.

This work was supported by the MAT2002-04178 grant from the CICYT. LFB wishes to thank Dr. H. Kunkel, Dr. F.J. Lázaro and Prof. O.V. Nielsen for their helpful advices.

References

1. C.M. Hurd, Contemp. Phys. **23**, 469 (1992)
2. J.A. Mydosh, *Spin Glasses: an experimental introduction* (Taylor & Francis, London, 1993)
3. T.J. Hicks, *Magnetism in Disorder* (Clarendon Univ. Press, Oxford, 1995)
4. J.L. Dormann, D. Fiorani, E. Tronc, Adv. Chem. Phys. **98**, 283 (1997)
5. J.A. De Toro, M.A. López de la Torre, M.A. Arranz, J.M. Riveiro, J.L. Martínez, P. Palade, G. Filloti, Phys. Rev. B **64**, 94438 (2001)
6. D.H. Ucko, Q.A. Pankhurst, L. Fernández Barquín, J. Rodríguez Fernández, S.F.J. Cox, Phys. Rev. B **64**, 104433 (2001)
7. T. Kaneyoshi, *Introduction to amorphous magnets* (World Sci., Singapore, 1992)
8. D.H. Ryan, J.M.D. Coey, E. Batalla, Z. Altounian, J.O. Ström-Olsen, Phys. Rev. B **35**, 8630 (1987)
9. Y. Obi, L.C. Wang, R. Motsay, D.G. Onn, M. Nose, J. Appl. Phys. **53**, 2304 (1982)
10. S.N. Kaul, Phys. Rev. B **27**, 6923 (1983)
11. S.N. Kaul, J. Phys.: Condens. Matter **3**, 4027 (1991)
12. H. Ma, H.P. Kunkel, G. Williams, J. Phys.: Condens. Matter **3**, 5563 (1991)
13. D. Kaptas, T. Kemény, L.F. Kiss, J. Balogh, L. Gránásy, I. Vincze, Phys. Rev. B **46**, 6600 (1992)
14. M. Ghafari, R.K. Day, J.B. Dunlop, A.C. McGrath, J. Magn. Magn. Mater. **104-107**, 1668 (1992)
15. N. Hegman, L.F. Kiss, T. Kemeny, J. Phys.: Condens. Matter **6**, L427 (1994)
16. I. Vincze, D. Kaptás, T. Kemeny, L.F. Kiss, J. Balogh, Phys. Rev. Lett. **73**, 496 (1994)
17. L.F. Kiss, T. Kemeny, I. Vincze, L. Granasy, J. Magn. Magn. Mat. **135**, 161 (1994)
18. H. Ren, D.H. Ryan, Phys. Rev. B **51**, 15885 (1995)
19. L. Fernández Barquín, J.C. Gómez Sal, S.N. Kaul, J.M. Barandiarán, P. Gorria, J.S. Pedersen, R. Heenan, J. Appl. Phys. **79**, 5146 (1996)
20. L.F. Kiss, T. Kemény, I. Vincze, J. Phys.: Condens. Matter **9**, 10501 (1997)
21. D. Gómez Plaza, L. Fernández Barquín, J. García Soldevilla, R. Antras, J.C. Gómez Sal, Sol. St. Comm. **102**, 353 (1997)
22. J. Nogués, K.V. Rao, J. Magn. Magn. Mater. **135**, L11 (1994)
23. J. Van Lierop, D.H. Ryan, Phys. Rev. Lett. **86**, 4390 (2000)
24. A. Fujita, H. Komatsu, K. Fukamichi, T. Goto, J. Phys.: Condens. Matter **5**, 3003 (1993)
25. H. Ren, D.H. Ryan, J. Appl. Phys. **73**, 5494 (1993)
26. D.H. Ryan, J.M.D. Coey, J.O. Ström-Olsen, J. Magn. Magn. Mater. **67**, 1668 (1987)
27. G.K. Nikolaides, G.C. Hadjipanayis, K.V. Rao, Phys. Rev. B **48**, 12759 (1993)
28. P.L. Paulose, V. Nagarajan, Phys. Rev. B **54**, 14934 (1996)
29. S.N. Kaul, P.D. Babu, J. Phys.: Condens. Matter **10**, 1563 (1998)
30. A. Perumal, V. Srinivas, K.S. Kim, S.C. Yu, V.V. Rao, R.A. Dunlap, Phys. Rev. B **65**, 64428 (2002)
31. M. Kopcewicz, A. Grabias, P. Nowicki, D.L. Williamson, J. Appl. Phys. **79**, 993 (1996)
32. A. Makino, T. Bitoh, A. Inoue, T. Masumoto, J. App. Phys. **81**, 2736 (1997)

33. A. Slawska-Waniewska, P. Nowicki, H.K. Lachowicz, P. Gorria, J.M. Barandiarán, A. Hernando, Phys. Rev. B **50**, 6465 (1994)
34. J.S. Garitaonandia, D.S. Schmool, J.M. Barandiarán, Phys. Rev. B **58**, 12147 (1998)
35. J.S. Garitaonandia, P. Gorria, L. Fernández Barquín, J.M. Barandiarán, Phys. Rev. B **61**, 6150 (2000)
36. J.M. Barandiarán, P. Gorria, I. Orue, M.L. Fdez-Gubieda, F. Plazaola, J.C. Gómez Sal, L. Fernández Barquín, L. Fournes, J. Phys.: Condens. Matter **9**, 5671 (1997)
37. T. Moyo, J. Magn. Magn. Mat. **154**, 201 (1996)
38. A. Slawska-Waniewska, M. Gutowski, H. Lachowicz, T. Kulik, H. Matyja, Phys. Rev. B **46**, 14594 (1992)
39. A. Perumal, V. Srinivas, A. Dhar, V.V. Rao, R.A. Dunlap, Phys. Stat. Sol. (a) **178**, 783 (2000)
40. A. Slawska-Waniewska, M. Pont, F.J. Lázaro, J.L. García, P. Nowicki, J.S. Muñoz, J. Magn. Magn. Mater. **140-144**, 453 (1995)
41. H. Tange, T. Matsuyama, A. Chikazawa, K. Konishi, T. Kamimori, J. Magn. Magn. Mat. **177-181**, 125 (1998)
42. K. Jonason, J. Matsson, P. Norblad, Phys. Rev. B **53**, 6507 (1996)
43. A. Hernando, P. Crespo, F.J. Castaño, J. Arcas, M. Multigner, J.M. Barandiarán, L. Fernández Barquín, Phys. Rev. B **61**, 3219 (2000)
44. J.S. Kouvel, M.E. Fisher, Phys. Rev. **136**, 1626 (1964)
45. S.N. Kaul, J. Magn. Magn. Mat. **53**, 5 (1985)
46. G. Sinha, A.K. Majumdar, J. Magn. Magn. Mat. **185**, 18 (1998)
47. K. Balakrishnan, S.N. Kaul, Phys. Rev. B **65**, 134412 (2002)
48. R.I. Bewley, R. Cywinski, Phys. Rev. B **54**, 15251 (1996)
49. J. Souletie, J.L. Tholence, Phys. Rev. B **32**, 516 (1985)
50. M. Fahnle, J. Souletie, J. Phys. C **17**, L469 (1984)
51. I. Skorvánek, S. Skwirblies, J. Kötzler, Phys. Rev. B **64**, 18437 (2001)
52. D. Li, Y. Shiokawa, Y. Haga, E. Yamamoto, Y. Onuki, J. Phys. Soc. Jpn **71**, 418 (2002)
53. A. Ogielski, I. Morgenstern, Phys. Rev. Lett. **54**, 928 (1985)
54. P.C. Hohenberg, B.I. Halperin, Rev. Mod. Phys. **49**, 435 (1977); S. Geschwind, D.A. Huse, G.E. Devlin, Phys. Rev. B **41**, 4854 (1990)
55. S.C. Bhargawa, A.H. Morrish, H. Kunkel, Z.W. Li, J. Phys.: Condens. Matter **12**, 9667 (2000)
56. M. Suzuki, Prog. Theo. Phys. **58**, 1151 (1977)
57. T. Bitoh, K. Ohba, M. Takamatsu, T. Shirane, S. Chikazawa. J. Magn. Magn. Mat. **154**, 59 (1996)
58. S. Mukherjee, R. Ranganathan, S.B. Roy, Phys. Rev. B **50**, 1084 (1994)
59. T. Bitoh, K. Ohba, M. Takamatsu, T. Shirana, S. Chikazawa, J. Magn. Magn. Mater. **154**, 59 (1996)
60. D. Fiorani, A.M. Testa, E. Agostinelli, P. Imperatori, R. Caciuffo, D. Rinaldi, P. Tiberto, F. Vinai, P. Allia, J. Magn. Magn. Mat. **202**, 123 (1999)
61. D.H. Ryan, A.D. Beath, E. McCalla, J. Van Lierop, J.M. Cadogan, Phys. Rev. B **67**, 104404 (2003)
62. D.X. Chen, V. Skumryev, J.M.D. Coey, Phys. Rev. B **53**, 15014 (1996)
63. V. Tsurkan, J. Hemberger, M. Klemm, S. Klimm, A. Loidl, S. Horn, R. Tidecks, J. Appl. Phys. **90**, 4639 (2001)
64. E.M. Levin, V.K. Pecharsky, K.A. Gschneidner Jr, J. Appl. Phys. **90**, 6255 (2001)
65. L.F. Kiss, T. Kemény, I. Vincze, L. Gránásy J. Magn. Magn. Mater. **135**, 161 (1994)
66. A.R. Wildes, J.R. Stewart, N. Cowlam, S. Al-Heniti, L.F. Kiss, T. Kemeny. J. Phys.: Condens. Matter **15**, 675 (2003)
67. L. Karlsson, R.L. McGreevy, J.D. Wicks. J. Phys.: Condens. Matter **11**, 9249 (1999)
68. J. Li, Z.L. Wang, T.C. Hufnagel, Phys. Rev. B **65**, 144201 (2002)
69. J.S. Garitaoandia, D.S. Schmool, J.M. Barandiarán, Phys. Rev. B **58**, 12147 (1998)
70. J. Arcas, A. Hernando, J.M. Barandiarán, C. Prados, M. Vázquez, P. Marín, A. Neuweiler. Phys. Rev. B **58**, 5193 (1998)
71. S. Morup, F. Bodker, P.V. Hendriksen, S. Linderoth, Phys. Rev. B **52**, 287 (1995)
72. C. Djurberg, P. Svedlindh, P. Norblad, M.F. Hansen, F. Bodker, S. Morup. Phys. Rev. Lett. **79**, 5154 (1997)
73. M.F. Hansen, P.E. Jönsson, P. Norblad, P. Svendinhl, J. Phys.: Condens. Matter **14**, 4901 (2002)
74. A. Hernando, E. Navarro, M. Multigner, A.R. Yavari, D. Fiorani, M. Rosenberg, G. Filoti, R. Caciuffo, Phys. Rev. B **58**, 5181 (1998)
75. E. Obradó, A. Planes, B. Martínez, Phys. Rev. B **59**, 11450 (1999)